

Bright Visible-Infrared Light Emitting Diodes Based on Hybrid Halide Perovskite with Spiro-OMeTAD as a Hole-Injecting Layer

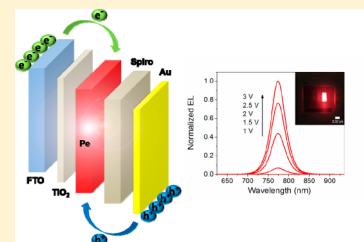
Oscar A. Jaramillo-Quintero,^{†,‡} Rafael S. Sanchez,[†] Marina Rincon,[‡] and Ivan Mora-Sero^{*,†}

[†]Photovoltaic and Optoelectronic Devices Group, Departament de Física, Universitat Jaume I, 12071 Castelló, Spain

[‡]Instituto de Energías Renovables, Universidad Nacional Autónoma de México, Apartado Postal 34, Temixco, Morelos 62580, México

Supporting Information

ABSTRACT: Hybrid halide perovskites that are currently intensively studied for photovoltaic applications, also present outstanding properties for light emission. Here, we report on the preparation of bright solid state light emitting diodes (LEDs) based on a solution-processed hybrid lead halide perovskite (Pe). In particular, we have utilized the perovskite generally described with the formula $\text{CH}_3\text{NH}_3\text{PbI}_{3-x}\text{Cl}_x$ and exploited a configuration without electron or hole blocking layer in addition to the injecting layers. Compact TiO_2 and Spiro-OMeTAD were used as electron and hole injecting layers, respectively. We have demonstrated a bright combined visible-infrared radiance of $7.1 \text{ W}\cdot\text{sr}^{-1}\cdot\text{m}^{-2}$ at a current density of $232 \text{ mA}\cdot\text{cm}^{-2}$, and a maximum external quantum efficiency (EQE) of 0.48%. The devices prepared surpass the EQE values achieved in previous reports, considering devices with just an injecting layer without any additional blocking layer. Significantly, the maximum EQE value of our devices is obtained at applied voltages as low as 2 V, with a turn-on voltage as low as the Pe band gap ($V_{\text{turn-on}} = 1.45 \pm 0.06 \text{ V}$). This outstanding performance, despite the simplicity of the approach, highlights the enormous potentiality of Pe-LEDs. In addition, we present a stability study of unsealed Pe-LEDs, which demonstrates a dramatic influence of the measurement atmosphere on the performance of the devices. The decrease of the electroluminescence (EL) under continuous operation can be attributed to an increase of the non-radiative recombination pathways, rather than a degradation of the perovskite material itself.



Solid state light emitting diodes (LEDs) have attracted much attention over the last decades, mainly due to the need of producing more energy efficient devices by means of low-cost procedures and materials. However, these devices are generally prepared from crystalline semiconductors, which demand high temperature, high vacuum, and time-consuming methodologies, thus increasing the final cost of the product and being unsuitable, for instance, for large-area displays.^{1,2} Therefore, great efforts are being devoted toward the search of new materials that must possess excellent electro-optical properties, while involving simple deposition procedures and/or mild crystal growth conditions, in order to reduce the production cost. Hybrid halide perovskite (Pe) match excellently with these material requirements and their derivatives have emerged as a very promising wide family of materials that can be exploited for a broad range of optoelectronic applications; including high performance photovoltaics,^{3–7} photodetectors,⁸ amplifier active devices,^{9–12} and light emitting diodes.^{13–17} The huge range of application of the perovskite materials rely on the unprecedented properties observed from their physical characterization. More specifically, perovskite structures have shown unique properties, such as high light absorption coefficient and room temperature photoluminescence on film,^{18,19} tunable light absorption and emission,^{14,20–22} long-range electron–hole diffusion lengths,^{23–25} ferroelectricity,^{26,27} among others. Very recent works have reported on the strong photoluminescent properties of lead halide perovskites,^{28,29} with photoluminescence quantum yields (PLQY) as high as

70% at high photon fluxes.²⁹ Therefore, these materials are envisaged to be ideal candidates for the development of high efficiency and cost-effective solution-processed light emitting diodes. In fact, hybrid halide perovskites were studied for this purpose at the end of the past century, and the EL was indeed demonstrated; however, the scarce works that could found in the literature involved complex nonsolution deposition procedures.^{30,31} The intensive work dedicated to the study of these materials, mainly due to their enormous potentiality for photovoltaic applications, and the progress made on the development of Pe-based devices in recent years, have successfully awaken the interest for using them as light emitters. Consequently, very recent works focused on the application of Pe for LEDs devices have emerged.^{13–17}

Here, we report on the preparation of visible-infrared bright light emitting diodes based on $\text{CH}_3\text{NH}_3\text{PbI}_{3-x}\text{Cl}_x$, which show high EQE values at a low applied voltage and a very low turn-on voltage. To do so, we have exploited a device configuration that has been successfully employed for the preparation of perovskite solar cells (PSCs). Very recently, Bolink and co-workers have shown that a PSCs prepared by evaporation with organic selecting contacts can exhibit also a good electroluminescence.¹³ In our approach, a fully solution processed device, with the exception of the evaporated Au contacts, has

Received: April 8, 2015

Accepted: May 1, 2015

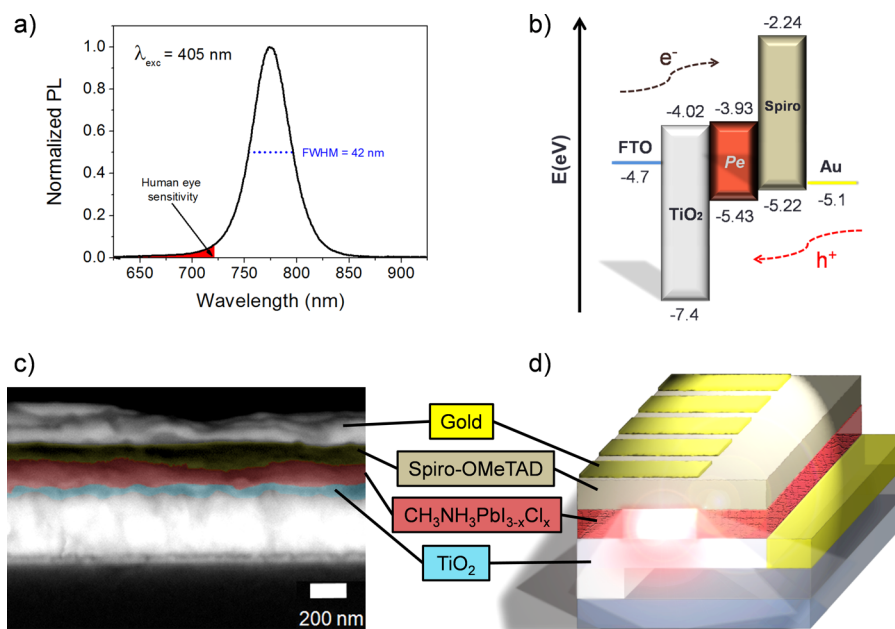


Figure 1. (a) Normalized photoluminescence spectrum of the $\text{CH}_3\text{NH}_3\text{I}_{3-x}\text{PbCl}_x$ film ($\lambda_{\text{exc}} = 405$ nm). The red area illustrates the wavelength range under the curve that the human eye has its major sensitivity.³² (b) Energy bands diagram of the materials employed for the preparation of the lead halide perovskite based LEDs. (c) Cross-section SEM image of a device showing the different layers: compact TiO_2 (cyan), perovskite (red), Spiro-OMeTAD (brown), gold (yellow). (d) Device configuration showing the different layers of materials with the active area highlighted.

been prepared. A thin TiO_2 film deposited by spray pyrolysis play a double role of electron injection layer (EIL) and hole blocking material. Conversely, a spin-coated Spiro-OMeTAD layer has been used as a hole injection layer (HIL) and electron blocking material. Therefore, our devices are prepared by sandwiching a spin-coated $\text{CH}_3\text{NH}_3\text{I}_{3-x}\text{PbCl}_x$ layer with different thicknesses between the two charge selective contacts. The thickness optimization of the light emitting layer (Pe) is crucial in order to allow confining a high concentration of charge carriers, i.e., electron–hole pairs, which must induce a high radiative charge recombination under biased charge injection.

Figure 1a shows the normalized photoluminescence spectrum, centered at 773 nm, of a perovskite thin film deposited on a FTO/ TiO_2 substrate. Conventionally, the visible spectrum is considered to be comprised between 390 and 720 nm. This is the range in which the eye sensitivity function is greater than 10^{-3} , considering that the maximum sensitivity at 555 nm is normalized to 1.³² The red area under the PL curve, Figure 1a, highlights the wavelength range where the human eye is more sensitive. Note that most of the light emitted by the prepared Pe corresponds to the near-infrared region (NIR). A strong PL signal has been observed from our films, thus evidencing weak nonradiative recombination pathways, as it has been previously reported.³³ This fact highlights the strong potentiality of this material for the development of optoelectronic devices. Actually, complete LED devices have been prepared by using the Pe film characterized in Figure 1a as a light-emitting layer.

Figure 1b illustrates the band energy diagram of the materials employed for the preparation of our devices; all values are indexed to the vacuum energy.³⁴ As it can be observed, the alignment of the energy position of the TiO_2 conduction band (-4.0 eV) is closely below the conduction band (CB) of Pe (-3.93 eV), while the valence band (VB) of Spiro-OMeTAD (-5.22 eV) is slightly above the valence band of Pe (-5.4 eV),

thus ensuring an efficient charge injection from both selective contacts into the light emitting material. Figure 1c,d shows a cross-section SEM image of a working device and a representation of the cell configuration, respectively, in which the different layers deposited are clearly highlighted. Hence, from the SEM image it is possible to estimate the thicknesses of the different layers: 60 nm TiO_2 (cyan), 150 nm Pe (red), 100 nm Spiro-OMeTAD (brown), and 60 nm gold (yellow). It is interesting to point out that our devices were fabricated on $\text{SnO}_2:\text{F}$ (FTO) substrates, as opposed to $\text{In}_2\text{O}_3:\text{SnO}_2$ (ITO) that is commonly employed in LED technology, including previously reported Pe-LEDs.^{13–17} FTO is significantly cheaper than ITO; however, it presents higher surface roughness. If the active layer has a pronounced thickness and roughness itself,³⁵ a significant deleterious effect due to the use of FTO is not expected. In our case, the Pe layer presents a relatively high thickness (see Supporting Information Figure S1), which dampens the effect of a rough substrate, thus allowing using FTO electrodes.

Those devices prepared based on the configuration shown in Figure 1c show a strong EL signal upon exceeding a low voltage threshold, as we discuss below. We optimized the thickness of the Pe layer, since thinner layers promote an increase of carrier density and consequently the radiative recombination, which enhance the performance of the ultimate device. Briefly, we deposited the perovskite layer by spin-coating a precursor solution, resulting from mixing 0.423 g (2.66 mmol) of $\text{CH}_3\text{NH}_3\text{I}$ (MAI), 0.246 g (0.88 mmol) of PbCl_2 and 1 mL of anhydrous DMF, at different spin rates (from 2000 to 5000 r.p.m.) (see experimental section for further details). As a general trend, thinner samples are obtained as the spin rates increases (see Figure S1). It is worth pointing out that other attempts of depositing thinner Pe layers by means of reducing the concentration of the precursor solution gave rise to poor stability devices that degraded very fast while measuring. This observation is probably ascribed to a low surface coverage when

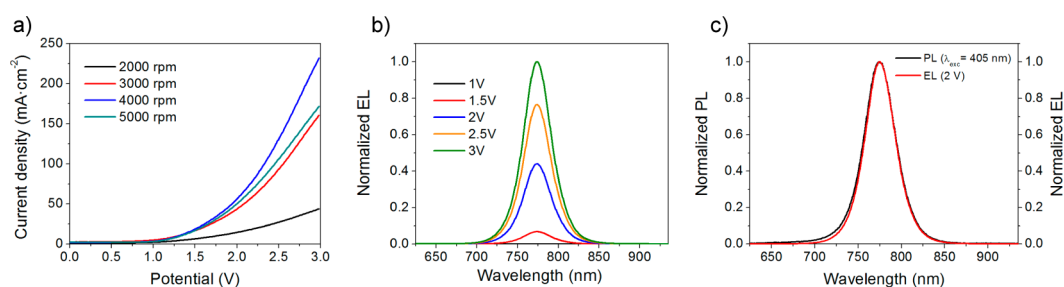


Figure 2. (a) Averaged J/V curves of a series of devices prepared by depositing the perovskite film under different spin-coating rates to control the thickness of the active layer. (b) Normalized electroluminescence at different forward applied potentials for a device containing a perovskite film deposited at 4000 r.p.m. (c) Plot of the normalized photoluminescence ($\lambda_{\text{exc}} = 405 \text{ nm}$) and the electroluminescence (2 V) signals.

depositing the Pe layer from a more diluted precursor solution. In addition, a similar effect was observed when the spin rate was increased beyond 5000 r.p.m.

Figure 2a shows the averaged J/V curves of the devices prepared at different spinning conditions, considering the forward and backward scans. As generally observed in perovskite solar cells under illumination, we have detected a strong hysteresis in the measured J/V curves under dark conditions. The as-measured J/V curves are plotted in Figure S2. Hysteresis phenomena have been reported by several authors in PSCs, and its exact origin is still under debate.^{36–39} From the averaged curves shown in Figure 2a, it is clearly observed that thicker Pe films are accompanied by a higher resistance, which means lower current density values at similar applied potentials. This trend is observed from 2000 to 4000 r.p.m. However, the resistance of the films prepared at 5000 r.p.m. increased. It is remarkable that all those samples prepared at the spin-coating conditions mentioned, showed EL upon the application of an external forward potential.

Pe films show a very narrow PL spectrum, with a low full width at half-maximum (fwhm) of 42 nm (Figure 1a), which ensures a pure color photoinduced emission. However, LEDs suffer in many cases from parasitic EL signals that arise from radiative recombination processes occurring not only in the bulk of the active material, but also at the interfaces or even in the electron–hole selective contacts. This effect usually limits the performance of the ultimate devices and causes significant modifications of the EL signal. Figure 2b shows the normalized EL intensity of a working device at different voltages. Since the electron (TiO_2) and hole (Spiro-OMeTAD) selective contacts employed here show excellent properties of hole and electron blocking layers, respectively, our devices do not suffer from additional radiative recombination pathways, thus showing a pure EL signal that matches perfectly with the PL spectra, as it can be clearly observed in Figure 2c.

Figure 3a shows the EQE values obtained for a series of samples with a different thickness of the Pe layer, where the highest values were obtained for the 4000 r.p.m. sample. In particular, the averaged EQE value obtained at our optimum Pe deposition conditions was 0.42% (0.48% for the record device) at a significantly low voltage (2 V) and current density ($56 \text{ mA}\cdot\text{cm}^{-2}$). The averaged values have been obtained from the measurement of nine different devices. A histogram of the EQEs can be found in Figure S3. Additionally, the radiance versus the applied potential of our devices is plotted in Figure 3b, which shows a mean value of $7.1 \text{ W sr}^{-1}\cdot\text{m}^{-2}$ ($7.7 \text{ W sr}^{-1}\cdot\text{m}^{-2}$ for the record device) at 3 V ($232 \text{ mA}\cdot\text{cm}^{-2}$). Therefore, our approach that consists on using TiO_2 and spiro-OMeTAD as injecting layers, demonstrates an almost 2-fold improvement

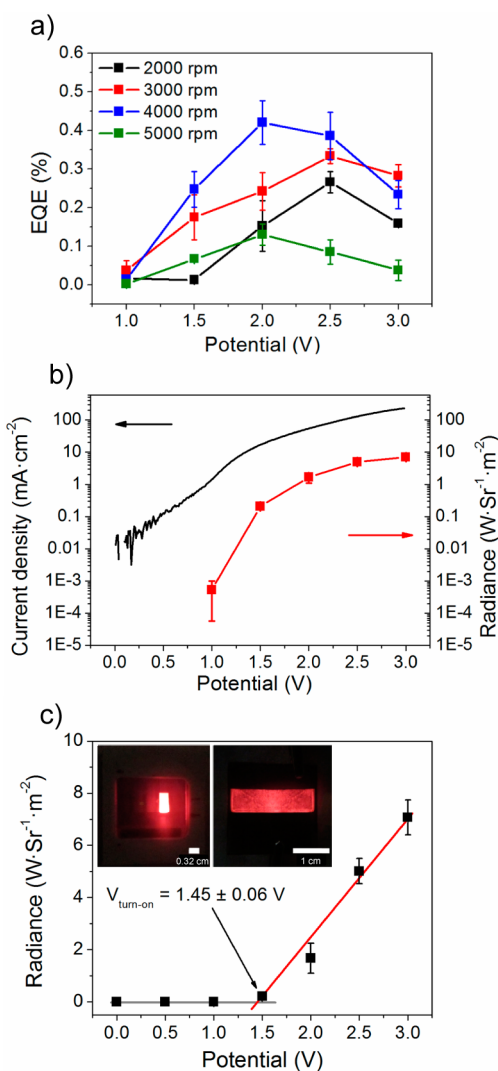


Figure 3. (a) EQEs of the devices at the different applied potentials depending on the different deposition rate of the perovskite films. (b) Current density and radiance in log scale of the devices prepared at 4000 r.p.m. versus the applied potential. (c) Radiance of the 4000 r.p.m. devices versus the applied potential. The onset shows a turn-on voltage of $1.45 \pm 0.06 \text{ V}$ (estimated from the red line linear fitting). The inset images show two working devices of different area (0.224 and 1.54 cm^2 , respectively) at 2 V forward applied bias.

of the maximum EQE and a similar maximum radiance value compared to similar devices reported in other works,^{15–17} at significantly lower current densities. Nevertheless, it is

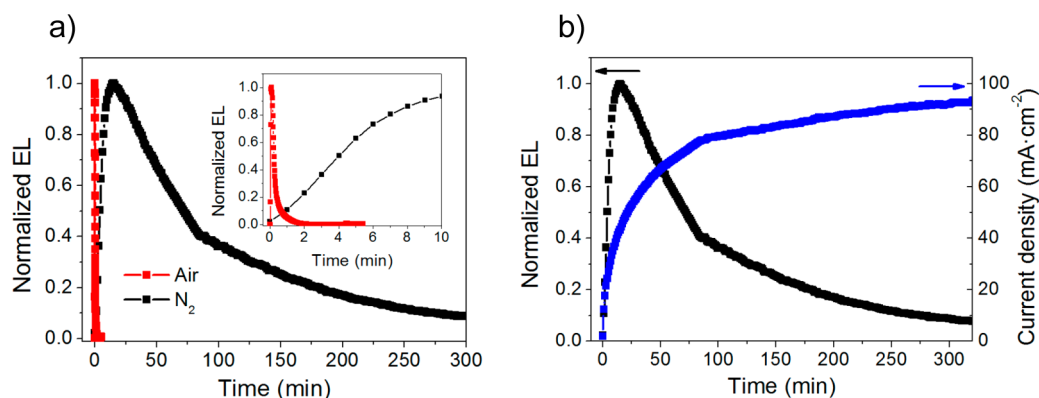


Figure 4. (a) Evolution of the normalized electroluminescence signal of a working device under air and nitrogen atmosphere at constant voltage (1.5 V). The inset shows the evolution of the signal at a shorter time-scale window. (b) Evolution of the electroluminescence signal and the current density under inert conditions.

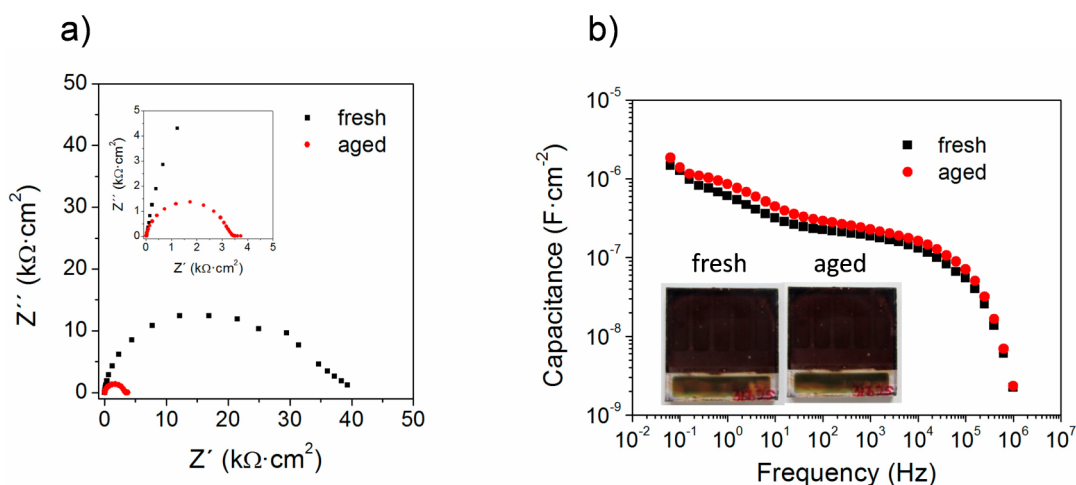


Figure 5. (a) Nyquist plot of the fresh and aged device at 0 V. (b) Bode plot of real capacitance before and after aging; inset: front picture of a fresh and aged sample.

important to remark that higher EQEs have been obtained for Pe LEDs but using a more sophisticated configuration with blocking layers in addition to injecting layers. Tan et al. exploited a much more sophisticated configuration (ITO/TiO₂/Al₂O₃(1 nm)/CH₃NH₃PbI_{3-x}Cl_x/F8/MoO₃/Ag), with the Al₂O₃ hole blocking layer prepared by atomic layer deposition, which presents an EQE of 0.76% for an applied bias of ~7 V.¹⁶ However, this device shows an EQE lower than 0.02% at 2 V. On the other hand, a very recent work published by Wang et al. reports a device configuration (ITO/ZnO-PEI/CH₃NH₃PbI_{3-x}Cl_x/TFB/MoO_x/Au) that shows very high EQE (3.5%) and radiance (28 W·sr⁻¹·m⁻²) values at 2.2 V (160 mA·cm⁻²), by applying a surface treatment of the ZnO with polyethylenimine (PEI) for improving the ZnO/Pe interface.⁴⁰ The outstanding results reported by Tan et al.,¹⁶ Wang et al.,⁴⁰ and our results here reported point to the improvement of the efficiencies of the Pe-LED by reducing the Pe layer thickness, while ensuring a full and homogeneous surface coverage in order to avoid short-circuits or preferential current pathways. In our case, the preparation of continuous Pe layers is limited to a relative high thickness of 150 nm (Figure S1 and S4). It could be anticipated that an improvement of the deposition method should yield thinner and flatter continuous layers, and consequently higher emission efficiencies of the Pe-

LEDs. In addition, the use of a blocking layer can also further move the emission efficiencies here reported.

Figure 3b shows the current density and radiance values (both in log-linear scale) versus the applied potential of those devices prepared by depositing the Pe layer at 4000 r.p.m. The log-linear J/V curve (black) clearly reveals an abrupt increase of the current density within the potential range comprised between 1 and 1.5 V, which is accompanied by a sudden increase of the radiance values. Therefore, this behavior indicates that the turn-on voltage corresponds to a value comprised within the mentioned potential range. Figure 3c shows the radiance values versus the applied potential in linear-linear scale. From the linear fitting of the radiance values, we have roughly estimated the turn-on voltage, that is as low as the Pe bandgap ($E_g \approx 1.5$ eV).³⁴ As it was shown above (Figure 1a), most of the light emitted by our devices is located in the NIR range where the human eye is not sensitive. In fact, only the 3% of the area under the PL spectrum correspond to the range of visible light where the human eye has the highest sensitivity; in spite of this, our devices show a strong red emission visible at naked eye, as it can be observed in the insets of Figure 3b, which corroborates the high brightness of the here reported light emitting diodes. Very importantly, by exploiting our methodology and device configuration, we were able to

prepare large area devices (area > 1.5 cm²) with a comparable performance and brightness (inset, Figure 3b).

In addition to the performance of the devices in terms of efficiency, brightness, and related parameters, we have carefully analyzed the stability of the unsealed Pe-based devices under continuous operation at constant voltage. These measurements were carried out by using a sample holder adapted for spreading a continuous nitrogen flux. As far as we know, this is the first study of stability of Pe-LEDs. As it was expected, oxygen seems to play a role on the stability of these devices. In particular, we applied a constant voltage of 1.5 V, while measuring the EL intensity over the time. Figure 4a shows the evolution of the EL signal at a constant potential under air (no gas flow) and under continuous N₂ flow. It is clearly observed that the sample working under air conditions suffers from a fast quenching of the EL signal; in fact, a 50% signal drop is observed after few seconds and disappears completely after 2 min. However, under inert conditions, the EL signal decreases significantly more slowly, and the emitted light can be detected even after 300 min under continuous operation. Perovskite degradation is conventionally detected by a change in the Pe layer absorption, which varies the sample color from dark brown to a yellowish color as the material degrades.^{41,42} In the case of Pe-LEDs here reported, including those samples measured under air and under inert atmosphere, the decrease of the EL under continuous operation could not be associated with the perovskite layer degradation, since no color change of the Pe layer is observed within the measured time scales (see Figure 5b). In addition, the EL signal increases gradually but significantly during the first 15 min under inert atmosphere (Figure 4b, black line), which is also accompanied by an increase of the current density (blue line). Although we are not able to provide a robust explanation for this phenomenon so far, there are several processes that could be involved. In fact, it has been recently observed that Pe-based solar cell devices show electro-optical processes with characteristic slow dynamics (seconds to minutes time scale).^{43,44} Currently, these phenomena, e.g., hysteretic J/V curves,^{36–39} slow transient photovoltage and V_{oc} decays,^{36,43} and slow photocurrent decay,⁴⁵ among others, are not fully understood, but the presence of Pe is a common denominator for their observation. Therefore, these phenomena have been ascribed to presumptive properties of the Pe materials, i.e., a dielectric polarization of the crystal structure or halide migration; however, unambiguous demonstrations are still required for elucidating the real origin of the slow transient behavior.

After the first 15 min under constant bias, the EL signal starts to drop while the current density continues increasing progressively and seems to approach the saturation after 300 min. The loss of PL is not recovered if the external bias is switched off, thus pointing to an irreversible evolution of the device performance upon the application of a constant electric field. Therefore, Pe-LEDs presents a significantly different behavior in terms of stability compared to our previous results on quantum dot (QD)-LEDs.³⁵ For NIR-emitting QD-LEDs based on core–shell PbS/CdS QDs, the EL reduction was accompanied by a decrease of the measured current density, and it was practically recovered after ceasing the application of the external voltage and short circuiting the device contacts, thus pointing to a charge accumulation phenomenon.³⁵ Huang and co-workers reported a switchable photovoltaic effect on perovskite layers by poling the sample at relative low voltages.⁴⁴

They attribute this effect to ion drift in the Pe layer, but in contrast to our results, they observed a reversible response.

From our point of view, the preservation of the Pe-LEDs current, the apparent non-degradation of perovskite layer (see inset in Figure 5b), and the non-reversibility of the EL loss point to an increase of the non-radiative recombination. To further investigate the reasons that rule this characteristic behavior, we performed impedance spectroscopy (IS) measurements. IS is a characterization technique extensively used to investigate the physical processes, as recombination, occurring in optoelectronic devices.²⁰ Recombination can be analyzed through the recombination resistance (R_{rec}) defined as the reverse derivative of voltage as a function of the recombination current. Consequently, recombination rate is inversely proportional to R_{rec} .²⁰ Figure 5a shows the Nyquist plot (0 V) of a fresh device (black squares), and the same device aged upon application of 1.5 V during 300 min (red dots) under N₂ flow. It can be clearly observed that R_{rec} taken as the diameter of the semicircle feature,²⁰ is significantly reduced after aging: $R_{rec} \approx 40 \text{ k}\Omega\text{-cm}^2$ for the fresh sample and $R_{rec} \approx 3.5 \text{ k}\Omega\text{-cm}^2$ for the aged device. Reduction of R_{rec} implies an increase of the recombination rate. Taking into account the decrease of electroluminescence emission with aging, it can be concluded that aging produces an increase of non-radiative recombination. Furthermore, we have analyzed the capacitance extracted from the IS measurements; Figure 5b shows the real part of the capacitance versus the perturbation frequency for the fresh (black squares) and aged (red dots) samples, respectively. These measurements revealed that the capacitance does not change after aging. It is very likely that this capacitance is associated mainly with the Pe layer where recombination takes place. Under this assumption, we infer that perovskite does not suffer from degradation. For comparison, capacitance of fresh sample and sample degraded after 3 days under 1 sun illumination is plotted in Figure S5. After this period the original black color of the CH₃NH₃PbI₃ perovskite was lost and sample became yellow the characteristic color of PbI₂. This is not the effect observed in our study, see Figure 5b. In addition, no significant change of color was observed after aging. From these considerations, we can assert that the EL signal decreases after aging due to the efficient activation of the non-radiative processes in detriment of the radiative pathways. Moreover, the difference between the EL in air and nitrogen environment cannot be due to a pure Pe degradation. Spiro-OMeTAD is prone to be partially oxidized in the presence of additives, oxygen exposure, and/or voltage application.^{46,47} Under such conditions the conductivity of the spiro-OMeTAD layer is significantly improved along with charge injection. This is the reason why we believe that the EL signal increases in the initial instants upon application of the bias. Obviously, Spiro-OMeTAD oxidation is more favored in air conditions, which is in clear agreement with the faster evolution of the EL signal when comparing samples in air and under nitrogen flow, respectively (Figure 4a). However, after reaching a given doping threshold, partial or complete loss of the EL signal is observed, further research is necessary to identify the physical origin of this behavior.

In summary, we have obtained bright visible-infrared light emitting diodes based on Pe by exploiting a device configuration commonly employed for the development of solar cells. Despite this simple approximation without electron/hole blocking layers, the use of high roughness substrates and the preparation of relatively thick Pe layers, significant EQE

values have been obtained (0.42% in average, with a record of 0.48%). In addition, the color purity and the fact that large area devices are accessible constitute essential issues to be emphasized for the development of future technologies on the field of lighting and/or display panels. We have studied for the first time the stability of Pe-LEDs, and demonstrated that the performance of these devices is still limited under continuous operation due to the increase of non-radiative recombination pathways. The evolution of the EL signal is not reversible, and it cannot be associated with an evident Pe degradation, as demonstrated by the IS experiments. Darkening of EL is associated with an increase of non-radiative recombination. Devoting efforts toward the use of alternative hole selective materials in parallel with the study of the device sealing are crucial to overcome the current limitations for a conceivable future commercialization. These results highlight the enormous potentiality of hybrid halide perovskites for the development of efficient LEDs, although it can be clearly deduced that there is much room for a future improvement of these devices.

METHODS

TiO₂ Compact Layer. First, the FTO layer present on the glass substrates (Pilkington TEC15, 15 Ω/sq resistance) was partially etched by chemical treatment with zinc powder and HCl (2 M), cleaned with soap (Hellmanex) and deionized water, followed by sonication in a mixture acetone/ethanol (1:1 v/v) for 15 min. The cleaned FTO substrates were further treated with UV-O₃ for 20 min. The TiO₂ compact layer was then deposited on the substrates by spray pyrolysis at 450 °C using a solution of titanium diisopropoxide bis(acetylacetonate) solution (75% in 2-propanol, Sigma-Aldrich) diluted in ethanol (1:39 v/v) and compressed oxygen as carrier gas. After spraying the precursor solution, the substrates were sintered on a hot plate for 30 min at 450 °C. Then, the hot plate was turned off, and the samples were left to cool down to room temperature.

Perovskite LED Fabrication. The CH₃NH₃PbI_{3-x}Cl_x perovskite precursor solution (100 μL), which was prepared by mixing 0.423 g (2.66 mmol) of CH₃NH₃I, 0.246 g (0.88 mmol) of PbCl₂ and 1 mL of anhydrous DMF, was spin-coated onto the TiO₂ inside the glovebox at different spin rates (from 2000 to 5000 r.p.m.) for 60 s, followed by a thermal treatment at 100 °C on a hot plate for 30 min. Then, the films were annealed at 100 °C for an additional hour in an oven under air flow. The CH₃NH₃PbI_{3-x}Cl_x was prepared in our laboratory by following standard procedures²² and the PbCl₂ (99.999%) and DMF (anhydrous) were purchased from Sigma-Aldrich and used as received without any further purification.

In parallel, a solution consisting of 72.3 mg spiro-OMeTAD (2,2',7,7'-tetrakis(*N,N*-di-*p*-methoxyphenylamine)-9,9-spirofluorene) in 1 mL of chlorobenzene was prepared. This solution was mixed with 28.8 μL of 4-*tert*-butylpyridine and 17.5 μL of a stock solution of 520 mg/mL bis-(trifluoromethylsulfonyl)amine lithium salt and spin-coated onto the FTO/TiO₂/CH₃NH₃PbI_{3-x}Cl_x films at 4000 r.p.m. for 30 s under air conditions. Finally, 60 nm of gold were thermally evaporated in an ultrahigh vacuum chamber on top of the devices.

Characterization of Perovskite Films and LEDs. The morphology of the films were analyzed by scanning electron microscopy using a JEOL 7001F (FEG-SEM). The thicknesses of the layers deposited for the preparation of the complete devices were estimated from the cross-section SEM images.

The PL spectra of the Pe films were obtained by using a spectrophotometer based on a CCD detector (Andor-iDUS DV420A-OE) coupled with a spectrograph as a diffraction grating (Newport 77400). A commercial blue laser diode (405 nm, 319 mW·cm⁻²) was used as an excitation source and a long-pass glass filter (FGL400S) was employed to attenuate the excitation light contribution.

The current density–voltage (*J/V*) curves and the EL measurements were registered using the previously detailed spectrophotometer equipment synchronized with a potentiostat (Gamry Reference 3000) in dark conditions without any encapsulation, both under nitrogen (N₂ flow) and air conditions. The EQE measurements were performed by calibrating the optical equipment with a commercial GaAs infrared LED (model EL-23G, peak emission centered at λ_{max}=940 nm, 28.3 W·sr⁻¹·m⁻²).

IS measurements were carried out under dark conditions at 0 V by means of a GAMRY Reference 3000 potentiostat, by applying a 20 mV voltage perturbation over the constant applied bias with the frequency ranging between 1 MHz and 50 mHz.

Measurements have been carried out using a non-sealed sample holder. Sample holder has a connection in order to allow a continuum gas flow. For stability measurements no-gas and N₂ gas flow conditions were used.

ASSOCIATED CONTENT

Supporting Information

Dependence of the thickness of the perovskite layer versus the spin-coating rate, as-measured *J–V* curves, histogram of the EQE values, SEM images, and Bode plot of real capacitance for fresh and degraded perovskite. The Supporting Information is available free of charge on the ACS Publications website at DOI: 10.1021/acs.jpcllett.5b00732.

AUTHOR INFORMATION

Corresponding Author

*E-mail: sero@uji.es.

Notes

The authors declare no competing financial interest.

ACKNOWLEDGMENTS

This work was supported by the Universitat Jaume I (project 12I361.01/1), Spanish MINECO (project MAT2013-47192-C3-1-R). Financial support to projects PAPIIT-UNAM (IN106912), CONACyT-México (153270), and the fellowship given to O.A.J.-Q. by CONACyT-México are also acknowledged. Authors acknowledge E. J. Juárez-Perez for the capacitance measurements of fresh and degraded perovskite.

REFERENCES

- (1) Tian, P.; McKendry, J. J.; Gong, Z.; Zhang, S.; Watson, S.; Zhu, D.; Watson, I. M.; Gu, E.; Kelly, A. E.; Humphreys, C. J. Characteristics and Applications of Micro-Pixelated GaN-Based Light Emitting Diodes on Si Substrates. *J. Appl. Phys.* **2014**, *115*, 033112.
- (2) Wang, R.; Nguyen, H.; Connie, A. T.; Lee, J.; Shih, I.; Mi, Z. Color-Tunable, Phosphor-Free InGaN Nanowire Light-Emitting Diode Arrays Monolithically Integrated on Silicon. *Opt. Express* **2014**, *22*, A1768–A1775.
- (3) Kazim, S.; Nazeeruddin, M. K.; Grätzel, M.; Ahmad, S. Perovskite as Light Harvester: A Game Changer in Photovoltaics. *Ang. Chem., Int. Ed.* **2014**, *53*, 2812–2824.

- (4) Kim, H.-S.; Im, S. H.; Park, N.-G. Organolead Halide Perovskite: New Horizons in Solar Cell Research. *J. Phys. Chem. C* **2014**, *118*, 5615–5625.
- (5) Park, N.-G. Organometal Perovskite Light Absorbers Toward a 20% Efficiency Low-Cost Solid-State Mesoscopic Solar Cell. *J. Phys. Chem. Lett.* **2013**, *4*, 2423–2429.
- (6) Snaith, H. J. Perovskites: The Emergence of a New Era for Low-Cost, High-Efficiency Solar Cells. *J. Phys. Chem. Lett.* **2013**, *4*, 3623–3630.
- (7) Jeon, N. J.; Noh, J. H.; Yang, W. S.; Kim, Y. C.; Ryu, S.; Seo, J.; Seok, S. I. Compositional Engineering of Perovskite Materials for High-Performance Solar Cells. *Nature* **2015**, *517*, 476–480.
- (8) Dou, L.; Yang, Y.; You, J.; Hong, Z.; Chang, W.-H.; Li, G. Solution-Processed Hybrid Perovskite Photodetectors with High Detectivity. *Nat. Commun.* **2014**, *5*, 5404.
- (9) Deschler, F.; Price, M.; Pathak, S.; Klintberg, L.; Jarausch, D. D.; Higler, R.; Huettnner, S.; Leijtens, T.; Stranks, S. D.; Snaith, H. J.; et al. High Photoluminescence Efficiency and Optically-Pumped Lasing in Solution-Processed Mixed Halide Perovskite Semiconductors. *J. Phys. Chem. Lett.* **2014**, *5*, 1421–1426.
- (10) Kao, T. S.; Chou, Y.-H.; Chou, C.-H.; Chen, F.-C.; Lu, T.-C. Lasing Behaviors Upon Phase Transition in Solution-Processed Perovskite Thin Films. *Appl. Phys. Lett.* **2014**, *105*, 231108.
- (11) Xing, G.; Mathews, N.; Lim, S. S.; Yantara, N.; Liu, X.; Sabba, D.; Grätzel, M.; Mhaisalkar, S.; Sum, T. C. Low-Temperature Solution-Processed Wide-Wavelength-Tunable Perovskites for Lasing. *Nat. Mater.* **2014**, *13*, 476–480.
- (12) Chen, K.; Barker, A. J.; Morgan, F. L. C.; Halpert, J. E.; Hodgkiss, J. M. Effect of Carrier Thermalization Dynamics on Light Emission and Amplification in Organometal Halide Perovskites. *J. Phys. Chem. Lett.* **2014**, *6*, 153–158.
- (13) Gil-Escrig, L.; Longo, G.; Pertegas, A.; Roldan-Carmona, C.; Soriano, A.; Sessolo, M.; Bolink, H. J. Efficient Photovoltaic and Electroluminescent Perovskite Devices. *Chem. Commun.* **2015**, *51*, 569–571.
- (14) Hoye, R. L. Z.; Chua, M. R.; Musselman, K. P.; Li, G.; Lai, M.-L.; Tan, Z.-K.; Greenham, N. C.; MacManus-Driscoll, J. L.; Friend, R. H.; Credgington, D. Enhanced Performance in Fluorene-Free Organometal Halide Perovskite Light-Emitting Diodes Using Tunable, Low Electron Affinity Oxide Electron Injectors. *Adv. Mater.* **2015**, *27*, 1414–1419.
- (15) Kumawat, N. K.; Dey, A.; Narsimhan, K. L.; Kabra, D. Near Infrared to Visible Electroluminescent Diodes Based on Organometallic Halide Perovskites: Structural and Optical Investigation. *ACS Photonics* **2015**, *2*, 349–354.
- (16) Tan, Z.-K.; Moghaddam, R. S.; Lai, M. L.; Docampo, P.; Higler, R.; Deschler, F.; Price, M.; Sadhanala, A.; Pazos, L. M.; Credgington, D.; et al. Bright Light-Emitting Diodes Based on Organometal Halide Perovskite. *Nat. Nano.* **2014**, *9*, 687–692.
- (17) Kim, Y. H.; Cho, H.; Heo, J. H.; Kim, T. S.; Myoung, N.; Lee, C. L.; Im, S. H.; Lee, T. W. Multicolored Organic/Inorganic Hybrid Perovskite Light-Emitting Diodes. *Adv. Mater.* **2014**, *27*, 1248–1254.
- (18) Im, J.-H.; Lee, C.-R.; Lee, J.-W.; Park, S.-W.; Park, N.-G. 6.5% Efficient Perovskite Quantum-Dot-Sensitized Solar Cell. *Nanoscale* **2011**, *3*, 4088–4093.
- (19) Stoumpos, C. C.; Malliakas, C. D.; Kanatzidis, M. G. Semiconducting Tin and Lead Iodide Perovskites with Organic Cations: Phase Transitions, High Mobilities, and Near-Infrared Photoluminescent Properties. *Inorg. Chem.* **2013**, *52*, 9019–9038.
- (20) Suarez, B.; Gonzalez-Pedro, V.; Ripolles, T. S.; Sánchez, R. S.; Otero, L. A.; Mora-Sero, I. Recombination Study of Combined Halides (Cl, Br, I) Perovskite Solar Cells. *J. Phys. Chem. Lett.* **2014**, *5*, 1628–1635.
- (21) Eperon, G. E.; Stranks, S. D.; Menelaou, C.; Johnston, M. B.; Herz, L. M.; Snaith, H. J. Formamidinium Lead Trihalide: A Broadly Tunable Perovskite for Efficient Planar Heterojunction Solar Cells. *Energy Environ. Sci.* **2014**, *7*, 982–988.
- (22) Noh, J. H.; Im, S. H.; Heo, J. H.; Mandal, T. N.; Seok, S. I. Chemical Management For Colorful, Efficient, and Stable Inorganic–Organic Hybrid Nanostructured Solar Cells. *Nano Lett.* **2013**, *13*, 1764–1769.
- (23) Stranks, S. D.; Eperon, G. E.; Grancini, G.; Menelaou, C.; Alcocer, M. J.; Leijtens, T.; Herz, L. M.; Petrozza, A.; Snaith, H. J. Electron-Hole Diffusion Lengths Exceeding 1 Micrometer in an Organometal Trihalide Perovskite Absorber. *Science* **2013**, *342*, 341–344.
- (24) Xing, G.; Mathews, N.; Sun, S.; Lim, S. S.; Lam, Y. M.; Grätzel, M.; Mhaisalkar, S.; Sum, T. C. Long-Range Balanced Electron- and Hole-Transport Lengths in Organic–Inorganic $\text{CH}_3\text{NH}_3\text{PbI}_3$. *Science* **2013**, *342*, 344–347.
- (25) Gonzalez-Pedro, V.; Juarez-Perez, E. J.; Arsyad, W.-S.; Barea, E. M.; Fabregat-Santiago, F.; Mora-Sero, I.; Bisquert, J. General Working Principles of $\text{CH}_3\text{NH}_3\text{PbX}_3$ Perovskite Solar Cells. *Nano Lett.* **2014**, *14*, 888–893.
- (26) Nuraje, N.; Su, K. Perovskite Ferroelectric Nanomaterials. *Nanoscale* **2013**, *5*, 8752–8780.
- (27) Kutes, Y.; Ye, L.; Zhou, Y.; Pang, S.; Huey, B. D.; Padture, N. P. Direct Observation of Ferroelectric Domains in Solution-Processed $\text{CH}_3\text{NH}_3\text{PbI}_3$ Perovskite Thin Films. *J. Phys. Chem. Lett.* **2014**, *5*, 3335–3339.
- (28) Schmidt, L. C.; Pertegás, A.; González-Carrero, S.; Malinkiewicz, O.; Agouram, S.; Mínguez Espallargas, G.; Bolink, H. J.; Galian, R. E.; Pérez-Prieto, J. Nontemplate Synthesis of $\text{CH}_3\text{NH}_3\text{PbBr}_3$ Perovskite Nanoparticles. *J. Am. Chem. Soc.* **2014**, *136*, 850–853.
- (29) Deschler, F.; Price, M.; Pathak, S.; Klintberg, L. E.; Jarausch, D. D.; Higler, R.; Hüttner, S.; Leijtens, T.; Stranks, S. D.; Snaith, H. J.; et al. High Photoluminescence Efficiency and Optically Pumped Lasing in Solution-Processed Mixed Halide Perovskite Semiconductors. *J. Phys. Chem. Lett.* **2014**, *5*, 1421–1426.
- (30) Chondroudis, K.; Mitzi, D. B. Electroluminescence from an Organic–Inorganic Perovskite Incorporating a Quaterthiophene Dye within Lead Halide Perovskite Layers. *Chem. Mater.* **1999**, *11*, 3028–3030.
- (31) Mitzi, D. B.; Chondroudis, K.; Kagan, C. R. Organic–Inorganic Electronics. *IBM J. Res. Dev.* **2001**, *45*, 29–45.
- (32) Schubert, E. F. *Light-Emitting Diodes*; Cambridge University Press: Cambridge, U.K., 2006.
- (33) Yamada, Y.; Nakamura, T.; Endo, M.; Wakamiya, A.; Kanemitsu, Y. Photocarrier Recombination Dynamics in Perovskite $\text{CH}_3\text{NH}_3\text{PbI}_3$ for Solar Cell Applications. *J. Am. Chem. Soc.* **2014**, *136*, 11610–11613.
- (34) Kim, H.-S.; Lee, C.-R.; Im, J.-H.; Lee, K.-B.; Moehl, T.; Marchioro, A.; Moon, S.-J.; Humphry-Baker, R.; Yum, J.-H.; Moser, J. E.; et al. Lead Iodide Perovskite Sensitized All-Solid-State Submicron Thin Film Mesoscopic Solar Cell with Efficiency Exceeding 9%. *Sci. Rep.* **2012**, *2*, 591.
- (35) Sanchez, R. S.; Binetti, E.; Torre, J. A.; Garcia-Belmonte, G.; Striccoli, M.; Mora-Sero, I. All Solution Processed Low Turn-On Voltage Near Infrared LEDs Based on Core-Shell PbS – CdS Quantum Dots with Inverted Device Structure. *Nanoscale* **2014**, *6*, 8551–8555.
- (36) Sanchez, R. S.; Gonzalez-Pedro, V.; Lee, J.-W.; Park, N.-G.; Kang, Y. S.; Mora-Sero, I.; Bisquert, J. Slow Dynamic Processes in Lead Halide Perovskite Solar Cells. Characteristic Times and Hysteresis. *J. Phys. Chem. Lett.* **2014**, *5*, 2357–2363.
- (37) Kim, H.-S.; Park, N.-G. Parameters Affecting I–V Hysteresis of $\text{CH}_3\text{NH}_3\text{PbI}_3$ Perovskite Solar Cells: Effects of Perovskite Crystal Size and Mesoporous TiO_2 Layer. *J. Phys. Chem. Lett.* **2014**, *5*, 2927–2934.
- (38) Snaith, H. J.; Abate, A.; Ball, J. M.; Eperon, G. E.; Leijtens, T.; Noel, N. K.; Stranks, S. D.; Wang, J. T.-W.; Wojciechowski, K.; Zhang, W. Anomalous Hysteresis in Perovskite Solar Cells. *J. Phys. Chem. Lett.* **2014**, *5*, 1511–1515.
- (39) Unger, E. L.; Hoke, E. T.; Bailie, C. D.; Nguyen, W. H.; Bowring, A. R.; Heumüller, T.; Christoforo, M. G.; McGehee, M. D. Hysteresis and Transient Behavior in Current-Voltage Measurements of Hybrid-Perovskite Absorber Solar Cells. *Energy Environ. Sci.* **2014**, *7*, 3690–3698.
- (40) Wang, J.; Wang, N.; Jin, Y.; Si, J.; Tan, Z. K.; Du, H.; Cheng, L.; Dai, X.; Bai, S.; He, H.; et al. Interfacial Control Toward Efficient and

Low-Voltage Perovskite Light-Emitting Diodes. *Adv. Mater.* **2015**, *27*, 2311–2316.

(41) Aldibaja, F. K.; Badia, L.; Mas-Marza, E.; Sanchez, R. S.; Barea, E. M.; Mora-Sero, I. Effect of Different Lead Precursors on Perovskite Solar Cell Performance and Stability. *J. Mater. Chem. A* **2015**, *3*, 9194–9200.

(42) Christians, J. A.; Miranda Herrera, P. A.; Kamat, P. V. Transformation of the Excited State and Photovoltaic Efficiency of $\text{CH}_3\text{NH}_3\text{PbI}_3$ Perovskite upon Controlled Exposure to Humidified Air. *J. Am. Chem. Soc.* **2015**, *137*, 1530–1538.

(43) Bertoluzzi, L.; Sanchez, R. S.; Liu, L.; Lee, J.-W.; Mas-Marza, E.; Han, H.; Park, N.-G.; Mora-Sero, I.; Bisquert, J. Cooperative Kinetics of Depolarization in $\text{CH}_3\text{NH}_3\text{PbI}_3$ Perovskite Solar Cells. *Energy Environ. Sci.* **2015**, *8*, 910–915.

(44) Xiao, Z.; Yuan, Y.; Shao, Y.; Wang, Q.; Dong, Q.; Bi, C.; Sharma, P.; Gruverman, A.; Huang, J. Giant Switchable Photovoltaic Effect In Organometal Trihalide Perovskite Devices. *Nat. Mater.* **2015**, *14*, 193–198.

(45) Gottesman, R.; Haltzi, E.; Gouda, L.; Tirosh, S.; Bouhadana, Y.; Zaban, A.; Mosconi, E.; De Angelis, F. Extremely Slow Photoconductivity Response of $\text{CH}_3\text{NH}_3\text{PbI}_3$ Perovskites Suggesting Structural Changes under Working Conditions. *J. Phys. Chem. Lett.* **2014**, *5*, 2662–2669.

(46) Cappel, U. B.; Daeneke, T.; Bach, U. Oxygen-Induced Doping of Spiro-Meotad in Solid-State Dye-Sensitized Solar Cells and Its Impact on Device Performance. *Nano Lett.* **2012**, *12*, 4925–4931.

(47) Nguyen, W. H.; Bailie, C. D.; Unger, E. L.; McGehee, M. D. Enhancing the Hole-Conductivity of Spiro-OMeTAD without Oxygen or Lithium Salts by Using Spiro(TFSI)₂ in Perovskite and Dye-Sensitized Solar Cells. *J. Am. Chem. Soc.* **2014**, *136*, 10996–11001.